Salt intrusions providing a new geothermal exploration target for higher energy recovery at shallower depths

Daniilidis, Alexandros; Herber, Rien

Published in:
Energy

DOI:
10.1016/j.energy.2016.10.094

Publication date:
2017

Energy 118 (2017) 658–670

Contents lists available at ScienceDirect

Energy

journal homepage: www.elsevier.com/locate/energy

Salt intrusions providing a new geothermal exploration target for higher energy recovery at shallower depths

Alexandros Daniilidis*, Rien Herber

University of Groiningen, Energy and Sustainability Research Institute Groningen (ESRIG), Geo-Energy Group, Nijenborgh 4, P.O. Box 800, 9747 AG, Groningen, The Netherlands

ARTICLE INFO

Article history:
Received 14 July 2016
Received in revised form
18 October 2016
Accepted 23 October 2016
Available online 8 November 2016

Keywords:
Salt dome heat flow
Geothermal
Direct use
Numerical model
NE Netherlands
Proof of concept

ABSTRACT

Direct use of geothermal energy can present challenges of financial feasibility in a low-enthalpy setting. The average temperature gradients in sedimentary basins make it necessary to reach larger depths for meaningful heat production, thus increasing the drilling cost. Therefore, full realization of geothermal projects in low-enthalpy environments has been difficult and not widely deployed. The concept of harvesting the positive temperature anomalies caused by the increased heat conductivity of salt bodies could enable access to higher temperatures at a shallower depth, thus reducing the necessary depth of drilling. In a potential site in NE Netherlands, temperature differences of up to 25 °C close to the top of a salt body are modeled. Substantiating this concept we show that the energetic benefits can result to up to 40% more energy extracted, while the temperature recovery of the field is only prolonged by 13%. This opens up new possibilities for geothermal applications in sedimentary basins.

1. Introduction

The use of geothermal energy for industrial or domestic purposes has been the subject of scientific focus in various different contexts [1–3]. However, direct use of energy from low-enthalpy geothermal sources can present challenges for financial feasibility, especially in areas where shallow, high temperature conditions are absent. The average geothermal gradient in sedimentary basins and the economic competition with fossil fuels are the main reasons for these challenges. In sedimentary basins, drilling has been identified as the highest cost contributor for geothermal projects [4–7], whereas the possible thermal energy output is largely determined by local temperature gradients and reservoir characteristics [8]. The above-mentioned challenges could be overcome by harnessing the energy channelled through the high heat conductivity of salt bodies [9], giving rise to locally higher temperatures at shallower depths, thus reducing drilling costs. This principle could outline potential geothermal targets through regional models using data generated by the hydrocarbon industry. Uncertainty remains pertinent despite high data availability in mature hydrocarbon basins [10]. Nonetheless the use of such data has been exemplified in different geothermal contexts before as a means to identify geothermal potential [11]. In this paper we substantiate the concept of harvesting the positive thermal anomalies caused by the heat conductivity of salt in the Eemshaven area in the NE Netherlands.

Salt bodies have a lower density than most rocks below 500 m burial depth [9]. When pressure levels exceed the formation strength, salt behaves in a visco-plastic way [12]; through this process, called halokinesis, salt flows towards the surface creating various structural shapes [13]. After halokinesis took place in Permian (Zechstein) evaporite sequences in the North of the Netherlands [14,15], several salt intrusions and domes have formed [13].

In sedimentary basins away from tectonic plate margins and in the absence of significant crustal extension, the heat flow maintains its average continental plate values [16]. In such settings the geothermal gradient is dominated by conductive processes [17,18] if significant vertical heat convection through fracture systems is absent [19]. The importance of conduction in the temperature distribution has also been identified in regional studies within the Southern Permian Basin (SPB) [20,21]. Consequently, stratigraphic intervals with high conductivity are of major importance for the temperature field.

The thermal conductivity of salt is two to four times higher than

* Corresponding author. Tel.: +31 50 363 8636.
E-mail address: a.daniilidis@rug.nl (A. Daniilidis).

http://dx.doi.org/10.1016/j.energy.2016.10.094

that of non-evaporitic sediments [22–25]. Heat is preferentially channeled through the salt, creating positive temperature anomalies around the top of a dome and negative ones at its base [19,20,22,26–28].

Higher temperatures found at shallower depths could contribute to a more economically viable utilization of direct use geothermal heat, especially in the low enthalpy context of the Netherlands, which has an average geothermal gradient of 31.3 °C/km [29]. Salt bodies have been found to influence the temperature gradient of existing nearby gas production wells in the greater southern Permian Basin [19,25,26,28,30], as well as within the Netherlands [29]. Modelling of salt intrusions in Northern Germany, within the same basin, has also linked them to increased temperature levels [21].

However, most studies examine an areas of tenths [26,31], hundreds [21,25,28–30] and sometimes thousands [18] of km with the underlying layer geometry sometimes based on large regional models. Such models are very insightful and identify temperature field anomalies on a larger scale. Nonetheless studies at a smaller scale could highlight details that are either missed or not pronounced in large regional studies. Using high resolution 3D seismic data for the geometry modelling and constraining the simulations with a temperature map as a lower boundary can increase the resolution of the temperature field. Such smaller scale models can help bridge the gap between the large scale regional models and models targeted at field development.

In this research we substantiate the concept of harvesting higher temperatures at a shallower depth due to the increased heat conductivity of salt bodies. The energetic benefits and possible economic impact of a direct-use geothermal installation is showcased. To this end, 3D seismic data were used to delineate a salt body located in the North of the Netherlands above the currently producing Groningen gas field. Based on structural interpretation we have constructed a geological model of the salt body, covering an area of 5 km^2 at depths ranging from 1.6 to 2.0 km. At these depths, temperatures of ca. 65 °C are predicted based on the average geothermal gradient. Using the geological model the specific temperature field has been calculated, using five thermal conductivity scenarios for the lithostratigraphic units. Furthermore, the effect of the computed temperature field on the performance of a conceptual geothermal aquifer positioned at the top of the salt structure is analysed. Lastly, a comparison is made with an aquifer positioned in a standard geothermal gradient for the basin.

1.1. Background

The operator of the Groningen gasfield (NAM), provided the 3D Pre-Stack Depth Migrated (PSDM) reflection seismic data which were used for seismic interpretation. Crossline and inline interval is 25 m, the vertical sample interval is 4 m and the data reach to a depth of 4 km. The available seismic data extends over an area of 27 km by 26 km, but interpretation focusses on the harbour area where there is demand for heat (Fig. 1). Seismic interpretation was carried out on top and base horizons of the main geological units using Petrel (Schlumberger) supported by 3D autotracking (Fig. 2a).

Furthermore, borehole lithostratigraphic data from 63 nearby wells (see Appendix A), publicly available from NL Olie-en Gasportaal [32], were used to further constrain the geological model. To aid the interpretation of the salt, seismic attributes of Instantaneous Phase (Fig. 2b), Amplitude Contrast, Relative Acoustic Impedance, Variance and Chaos were computed from the original seismic dataset.

2. Structural model

2.1. Geology

In the area of interest a salt ridge was identified with a thickness of up to 1500 m (Fig. 3c). Within this area, the top of the salt exhibits a depth range between 1,600 m and 2,000 m covering circa 5 km^2 (Fig. 3b). The geometry of the salt dome tightly matches the regional model by Strozyk et al. (2014) for the Groningen High region. Furthermore, the shape of the salt ridge correlates strongly to the fault orientation in the underlying Rotliegend (Fig. 3d). The salt structure is up to circa 1,000 m thicker above the faulted Rotliegend basement, while it drops to its normal stratigraphic

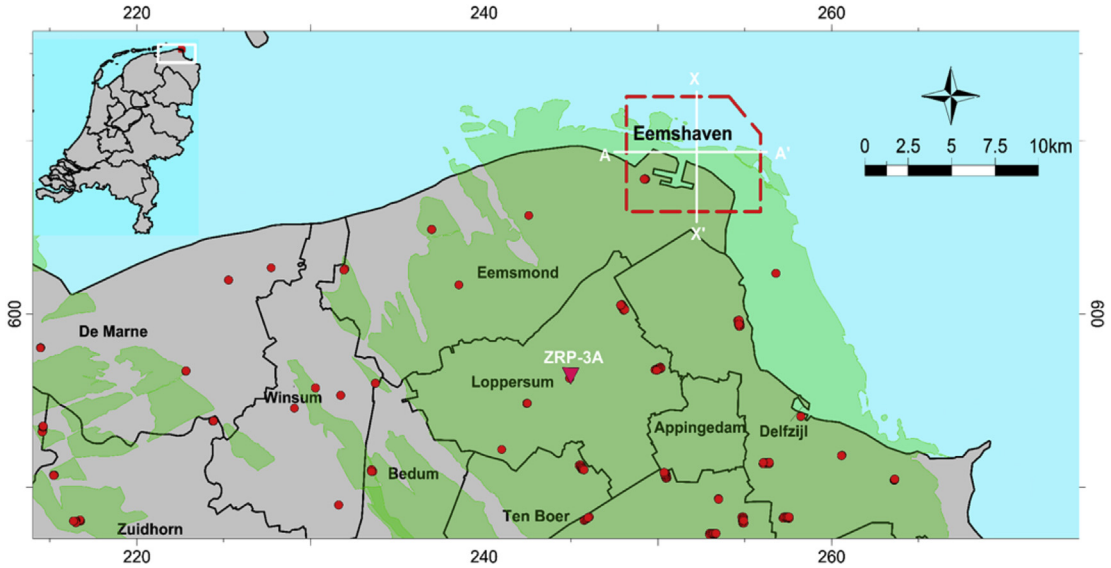

Fig. 1. Study area in the North of the Netherlands. Axes are based on RD-New system coordinates, converted to distance (km). Red dots depict surface locations of existing gas wells, the black lines depict municipal borders and the coast line and gas fields are indicated in light green. The dotted red line outlines the area of interest around the Eemshaven port, where demand for geothermal heat is present. The cross section X-X′ is presented in Fig. 2, and cross section A-A′ in Fig. 3. Distributed Temperature Sensing (DTS) data of the ZRP-3A well are presented in Fig. 6. (For interpretation of the references to colour in this figure legend, the reader is referred to the web version of this article.)

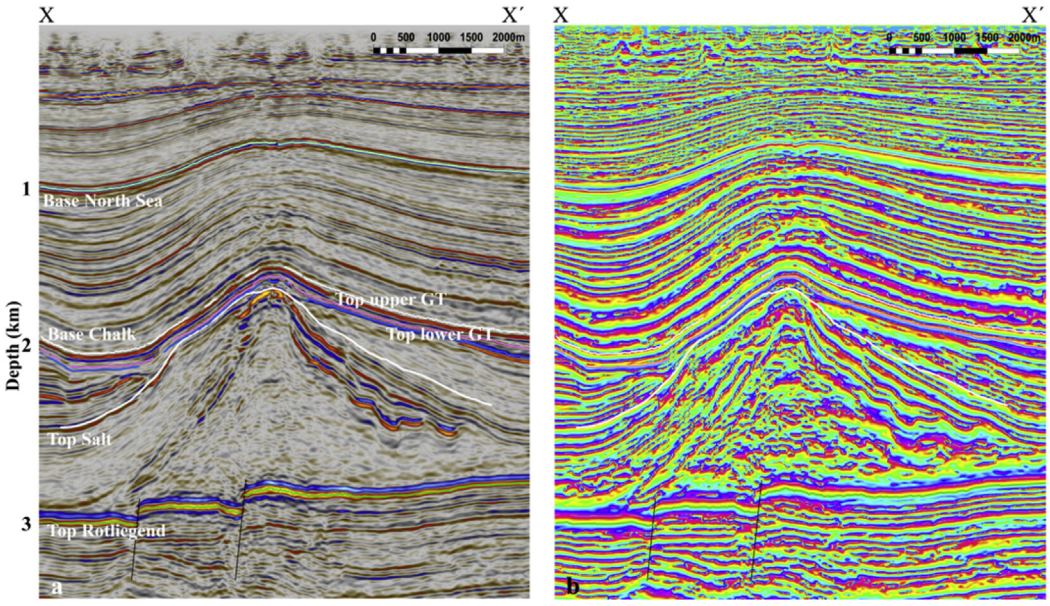

Fig. 2. Section X-X′ from Fig. 1 showing (a) seismic data and (b) instantaneous phase attributes. The abbreviation GT stands for the Germanic Trias group.

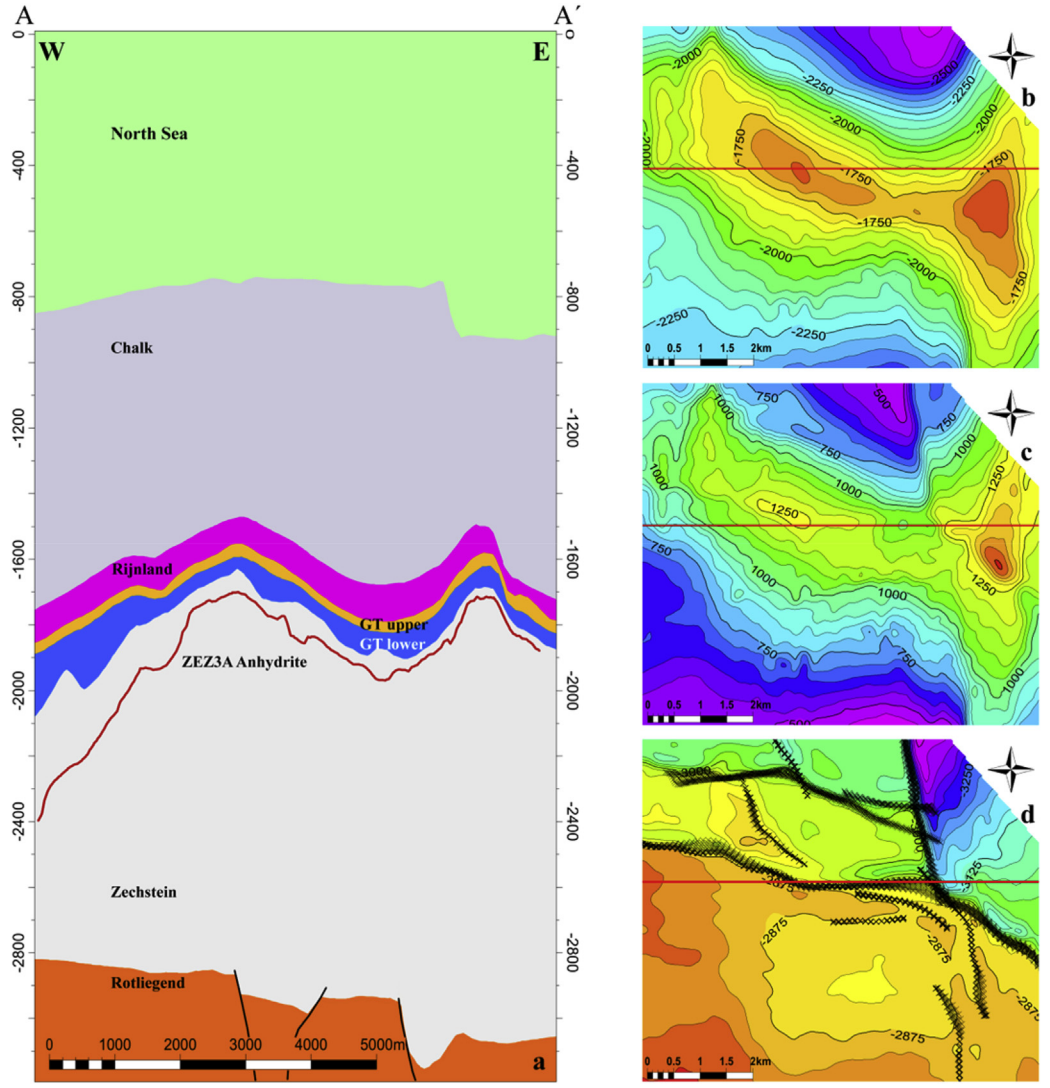

Fig. 3. (a) Geological cross-section (b) top salt depth map, (c) salt isochore thickness map and (d) top Rotliegend depth map. Red lines on figures (b, c, d) indicate the location of the cross section (a), while the x marks on figure (d) delineate Rotliegend faults. The area covered in figures b, c and d is highlighted by the red polygon in Fig. 1. The main orientation of the salt dome structure strongly correlates with the underlying Rotliegend faults (WWN-EES). The secondary elongated part of the dome on the east part of figure (b) also correlates with the faults oriented (NNW-SSE). Faults in the Rotliegend are considered to be of Jurassic age, related to the stress fields associated with opening up of the Atlantic Ocean [35]. Jurassic sediments are eroded at the Base Cretaceous unconformity, while there is another discontinuity between the lower Germanic Trias sediments and the underlying Zechstein salt. (For interpretation of the references to colour in this figure legend, the reader is referred to the web version of this article.)

thickness of 500 m–600 m away from the faults (Fig. 3c). The halokinetic process therefore appears to have been triggered by fault movements, which is often seen elsewhere in the basin [9,33,34].

The presence of an anhydrite layer was interpreted within the salt ridge (Fig. 3a). The layer was correlated with well data in the area and identified as the ZEZ3A formation. The anhydrite layer corroborates both the geometric shape, as well as the parallel to sub-parallel relation to the top of the salt in the area of the Groningen High; the anhydrite is closer to top salt in the upper parts of the salt body than on the sides [13]. Due to its strong seismic reflection signature, the layer can be used as a phantom where the top salt reflection is weak.

3. Simulation models

Two types of models are used for the simulations. First a steady state temperature model that calculates the temperature field using different heat conductivity scenarios. One of the heat conductivity scenarios is also simulated using a different grid for comparison purposes. Following this, and for each steady state temperature model, a sub-model is extracted representing the conceptual reservoir model. Each conceptual reservoir model uses three different production scenarios for energy generation through a doublet setup. The steady state temperature models in combination with the reservoir models provide an overview of the energy generation and reservoir behaviour in all the considered heat conductivity and production scenarios.

3.1. Steady state temperature model

A steady state model was built in the PetraSim/TOUGH2 [36] reservoir simulator. Two different grids were considered to rule out the influence of grid resolution to the results. Both models have been optimized to balance between resolution and computational time. To this end the findings of previous temperature studies were taken into account, where for conductive settings the mesh has been found convergent as long as it manages to resolve the structural complexity [30]. Fig. 4 illustrates the ability of both models to capture the geometry in one of the most complex parts of the geological model. Horizontal discretization is 93 × 79 cells, while vertically the model extends from the top part of the Rotliegend to the surface, using the structural framework interpreted in Petrel. The horizons represent the major contacts between the lithostratigraphic groups. The characteristics of both models are presented in Table 1.

Heat conductivities for the lithostratigraphic units were based on literature from comparable temperature models and are summarized in Table 2. Five scenarios were devised (NOTSALT-MIN-MED-MAX-XTRM) to account for the variation of literature input. In

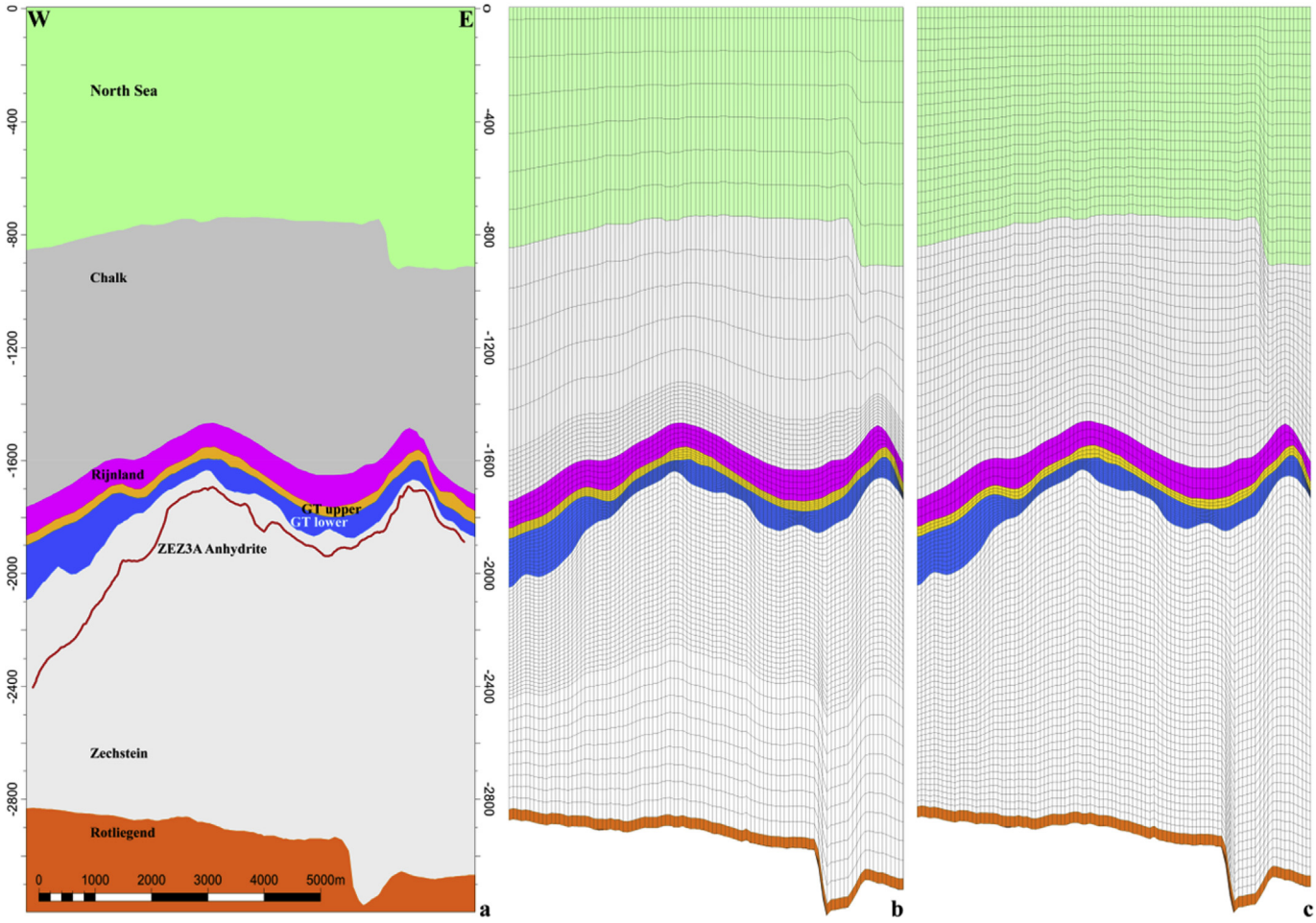

Fig. 4. Different meshes applied in the steady state models. The geological model constructed in Petrel (a) exhibits a complex geometry above the crest of the dome, as well as thickness variations of the overburden. Nonetheless both the grid 1 (b) and the grid 2 (c) models are able to capture these geometrical variations by closely outlining the changes in thickness. The scenarios were run using the grid 1 model, while the MIN scenario was also run using grid 2 for comparison.

Table 1
Architecture and characteristics of the steady state models. The PetraSim grid 1 uses higher vertical resolution around the top of the dome, while the grid 2 model ensures that there are no cells with a thickness larger than 50 m. The boundary condition at the base is derived from the temperature map of the top of the Rotliegend in the Groningen gas field [37]. Both models do not include faults and use the thermal inputs presented in Table 2, while their lithostratigraphic inputs and their hydraulic characteristics are presented in Table 3.

	PetraSim (TOUGH-MP)	
	Grid 1	Grid 2
Dimensions	6.9 km × 6.0 km x 3.3 km	
Horizontal discretization	75 m × 75 m (93 × 79 cells)	
Horizontal cell count	7270	7270
Layers	87	103
Total cell count	623,790	747,162
Lithostratigraphic units	7	
Boundary condition top	Temperature (10 °C)	
Boundary condition base	Temperature (map)	

all scenarios, the model was allowed to reach a steady state temperature distribution constrained by the boundary conditions (Table 1). The structural characteristics of the models are identical for all simulations and only the heat conductivity values are different.

The hydraulic and thickness characteristics of the model layers are presented in Table 3. The top of the model is formed by ground level so that a temperature boundary condition can be applied. Any convection effects that would require a chemical species characterization to describe thermohaline flow [42] are beyond the focus of this study.

3.2. Conceptual reservoir model

The reservoir model has dimensions of 1.5 km by 1.7 km and uses a horizontal discretization of 75 m. Vertically, the model extends from the top of the Upper Germanic Trias down to 50 m inside the salt layer. The layer characteristics remain the same as the grid 1 steady state model (see Table 1). An overview of the model characteristics can be found in Table 4, while Fig. 5 shows the outline of the model in relation to the initial state models and the well locations.

The well positioning takes into account the geometry of the lower Germanic Trias reservoir and ensures as much as possible a continuous reservoir thickness (Fig. 5). The temperature distribution is also considered and therefore, the injector is positioned where the highest temperatures are encountered (see Fig. 7). Production is sustained for 50 years, after which the reservoir is allowed to recover.

4. Results and discussion

The results of the steady state temperature simulations are presented first. Following, a vertical temperature profile in two locations, a depth slice at the top of the salt ridge and the difference between heat conductivity scenarios on an N-S plane are discussed. Additionally the results of the dynamic reservoir simulations are discussed. In these, for each conductivity scenario the temperature at the middle layer of the reservoir model is plotted, followed by the producer well temperature over time.

Table 4
Overview of the conceptual reservoir model characteristics and the production scenarios.

Dimensions XY	2391 m by 1656 m
Depth	1553 m–2204 m
Reservoir thickness (min-avg-max)	24 m - 62 m - 170 m
Well separation at reservoir depth	995 m
Cell count	14,080
Production scenarios	100m^3/hr - 175m^3/hr - 250m^3/hr
Re-injection temperature	40 °C

Table 2
Heat conductivity values found in literature for temperature modelling studies in the greater area of the Netherlands and Germany and values for the lithostratigraphic groups used in the simulations. The data are sourced from: Set 1 [19], Set 2 [38], Set 3 [39], Set 4 [40], Set 5 [26] and Set 6 [41]. The extreme and NOTSALT scenarios are devised as the absolute limits that could be encountered. The NOTSALT scenario assumes medium values for all groups and a Zechstein group conductivity the same as the overlying Germanic Trias group. The extreme scenario assumes that all layers have the lowest values of heat conductivity while the Zechstein layers have the maximum. The MIN, MED and MAX scenarios use the respective data from the above listed sources.

Lithostratigraphic group	Literature thermal conductivity values (W/m K)						Simulation scenario values (W/m K)				
	Set 1	Set 2	Set 3	Set 4	Set 5	Set 6	NOTSALT	MIN	MED	MAX	XTRM
North Sea	–	–	–	–	–	2.3			2.3		
Chalk	1.9	1.8	2.8	1.9	–	2.2	2.1	1.8	2.1	2.8	1.8
Rijnland	2.0	2.0	3.0	2.0	–	2.5	2.3	2.0	2.3	3.1	2.0
Germanic Trias	2.0	2.2	2.0	2.0	–	2.8	2.2	2.0	2.2	3.7	2.0
Zechstein (salt)	3.5	4.5	–	3.5	5.5	3.1	2.2	3.1	4.0	5.5	5.5
Rotliegend	2.1	3.3	–	2.2	–	4.0	2.5	2.1	2.5	4.0	2.1

Table 3
Hydraulic and thickness values of the lithostratigraphic groups. Vertical permeability is an order of magnitude lower (10% of horizontal) than the respective horizontal permeability of each group [43]. The grid 1 model is not equidistant but is refined around the top of the salt dome (see Fig. 4).* a generic reservoir is assumed with a permeability representative of a sandstone body is used in order to evaluate the concept of harvesting the higher heat flow on top of the dome.

Lithostratigraphic group	Horizontal Permeability (mD)	Porosity (%)	Thickness (m)		Model layers	
			Min	Max	Grid 1	Grid 2
North Sea	101.3	10.00	671	1037	7	22
Chalk	0.1	10.00	492	1023	15	22
Rijnland	1.0	12.00	5	166	5	3
Germanic Trias upper	1.0	18.00	2	136	5	3
Germanic Trias lower*	101.3	18.00	1	482	13	11
Salt	1e-8	0.01	404	1551	40	41
Rotliegend	101.3	18.00	–		1	1

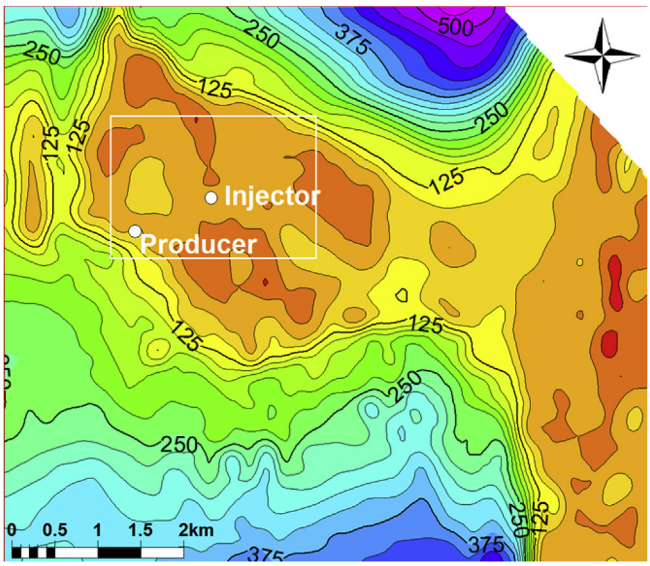

Fig. 5. Outline of the conceptual reservoir model boundaries, location of the injector and producer well and the thickness of the reservoir (lower Germanic Trias lithostratigraphic layer).

4.1. Steady state temperature simulations

Fig. 6 depicts the steady state temperature model results. The vertical temperature profiles are plotted at two different locations representing the highest (1227 m) and lowest thickness (497 m) of the Zechstein salt lithostratigraphic group (for overview see Fig. 7). The fixed top and bottom temperature boundaries constrain the possible temperature field solutions to identical top and bottom points for all scenarios in each location. Differences between scenario results stem from the thermal conductivity values used (see Table 2). Differences between locations can be attributed to geometrical (i.e. thickness) differences of the lithostratigraphic units.

In location 1 we observe two discrete parts of the temperature profile: a steep part through the salt interval and a less steep in the overlying sediments. The steep profile is caused by heat channeled to the surface faster due to the higher heat conductivity of salt and its large thickness in location 1. The two sections of the profile remain discrete for four of the thermal conductivity scenarios and their slopes change at the top of the salt. Only the NOTSALT scenario is not following this trend, due to the heat conductivity of the "salt" layer interval being similar to the overlying Germanic Trias sediments. No model differences between grid 1 and grid 2 are distinguishable, as the MIN and MINGRID datasets perfectly overlap. The XTRM scenario exhibits the highest temperature at the top of the salt, while the NOTSALT scenario exhibits the lowest. The difference between the XTRM and NOTSALT scenarios is up to

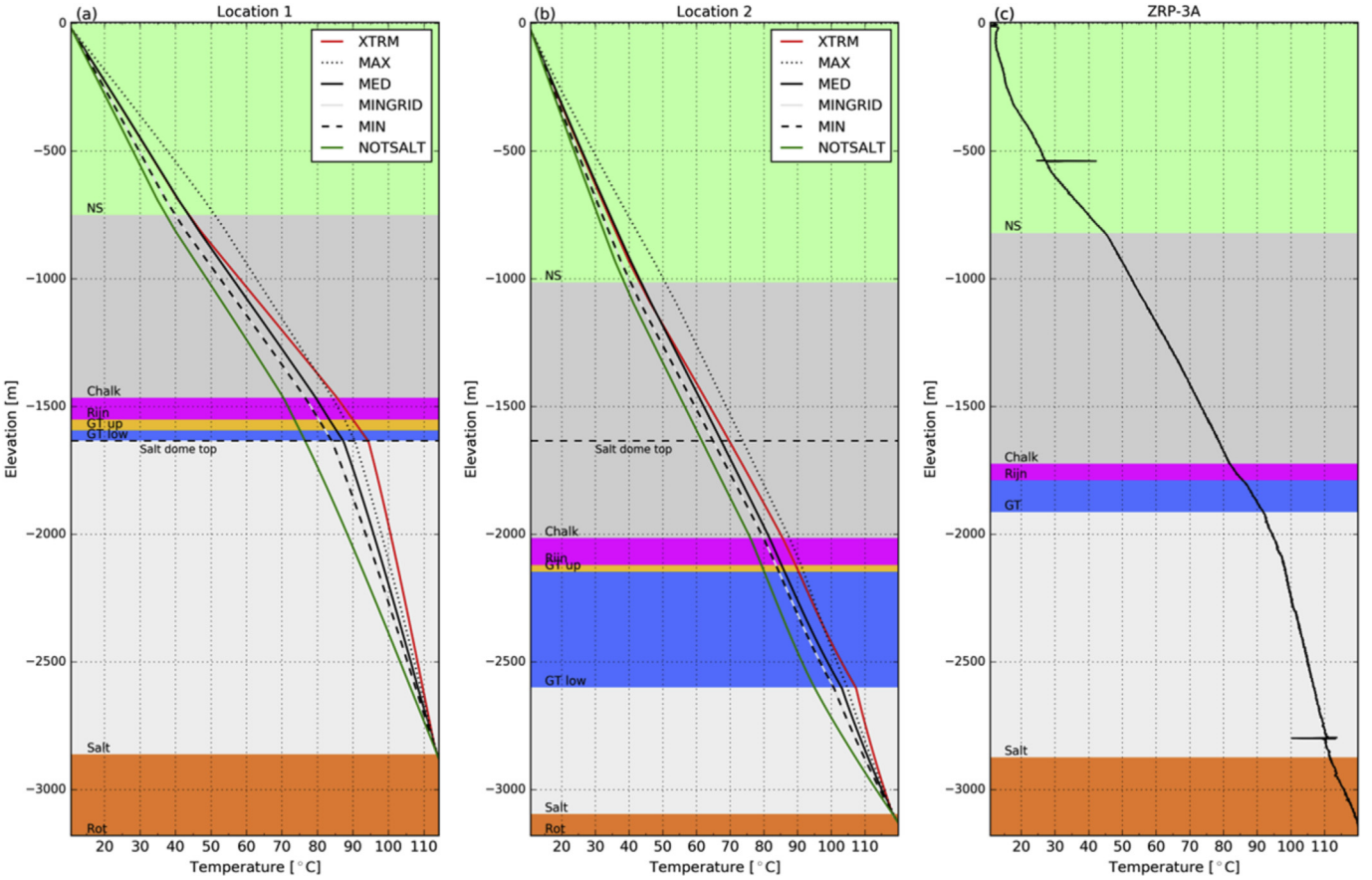

Fig. 6. Vertical temperature profile at the two locations highlighted in Fig. 7: (a) location 1, (b) location 2 and (c) DTS data from the ZRP-3A well. For ZRP-3A well location see Fig. 1. Background colour highlights the lithostratigraphic group intervals. All scenarios make use of grid 1 except for MINGRID that makes use of grid 2 (see Table 1). Temperature profiles in figures (a) and (b) stop at the top of the Rotliegend since that is the base boundary of the model. (For interpretation of the references to colour in this figure legend, the reader is referred to the web version of this article.)

~17 °C at the crest of the structure (Fig. 6a, see also Fig. 8c). Lastly, it is important to note that even though the XTRM scenario exhibits the highest temperature at the top of the salt, it results in lower temperature levels than the MAX scenario for depths shallower than ca. 1350 m. This result could be explained by the lower conductivity of the XTRM scenario layers above the salt compared to the MAX scenario, which leads to higher temperature contrast at the top of the salt but lower temperatures in the overlying layers.

In location 2 we see a much more linear temperature gradient irrespective of the thermal conductivity scenario. A small change in the angle of the temperature profile can be observed but it is not as pronounced as in location 1 (Fig. 6b). The stratigraphic thickness of the salt is not enough to create a distinct temperature anomaly in location 2. The scenarios show the same order in terms of temperature for a given depth as in location one. Notably, the MAX scenario exhibits higher temperatures than the XTRM scenario already at a depth of ca. 2350 m. The model differences between MIN and MINGRID are again not distinguishable, corroborating previous research where horizontal grid resolution was found to be more important than vertical resolution for the conductive field [30].

A temperature difference of circa 20 °C can be observed between the two locations for the same scenario at a depth of 1634 m (top of the dome at location 1) as seen in Fig. 6a&b. This difference can be attributed to the different salt thickness between the locations and is present for all conductivity scenarios (see also Fig. 7). Similar temperature levels as location 1 in areas where salt exhibits its bedded thickness (like location 2) are encountered 500–600 m deeper.

The ZRP-3A well, drilled as part of the Groningen gas field monitoring program, is situated 15 km away from our study area in the same geological setting. The well encounters a salt layer thickness of 960 m, which falls between the salt thickness of locations 1 and 2, but closer to location 1 (Fig. 6c). The Distributed Temperature Sensing (DTS) method provides high resolution temperature measurements with little uncertainties [44]. The ZRP-3A well DTS temperature measurements clearly depict the steeper temperature flow through the Zechstein layers. The steepness of the slope through the salt is between the MED and MAX scenarios for location 1.

Fig. 7 depicts the temperature of a depth slice at 1600 m (top part of the salt structure) for all conductivity scenarios. Locations 1 and 2 exhibit the highest and lowest temperatures respectively for all heat conductivity scenarios used (see also Fig. 6). Nonetheless, the temperature values at these locations differ. The NOTSALT (Fig. 7f) scenario represents the absence of the increased heat conductivity of the salt lithostratigraphic interval and can therefore be used as a basis for comparison. The other lithostratigraphic intervals of the NOTSALT scenario have average heat conductivity values (see Table 1).

For all scenarios the lower temperatures are situated in the areas of the lowest stratigraphic thickness of the salt lithostratigraphic group. The difference between the NOTSALT and the MIN, MED, MAX and XTRM scenario for low temperatures is 4 °C, 7 °C, 13 °C and 9 °C respectively (Fig. 7). The MAX scenario (Fig. 7b) exhibits higher temperatures than the XTRM (Fig. 7a) one, in this case in the areas of low stratigraphic salt thickness. This can be attributed to the contributions from the other layers being higher under the MAX scenario, since all layers use the maximum respective heat conductivity.

Compared to the NOTSALT scenario (Fig. 7f), the difference of the MIN, MED, MAX and XTRM scenarios for high temperatures is 7 °C, 10 °C, 14 °C and 17 °C respectively. In the areas around the top of the salt ridge (salt thickness > 1200 m) the temperature differences for all scenarios increase. For these high temperatures the XTRM scenario exhibits the biggest contrast with the NOTSALT base scenario.

Under the MAX heat conductivity scenario we observe a higher overall temperature throughout the domain for both low and high temperature locations compared to all other scenarios. The XTRM scenario only shows higher temperatures than the MAX scenario at the top of the salt structure. The temperature observed in the MIN scenario around location 2 (62 °C) is in line with the predicted temperature for this depth (~60 °C) for an average geothermal gradient of 31.3 °C/km [29] for North Netherlands. The differences between the MIN (Fig. 7e) and MINGRID (Fig. 7d) scenario is not more than 0.5 °C. Between these two scenarios some differences on the contours can be observed in the areas where the lower temperatures are encountered (around location 2), but the grid differences do not alter the overall temperature field.

At its lowest stratigraphic thickness (location 2) the salt causes a positive temperature anomaly between 4 °C (MIN scenario) and 13 °C (MAX scenario) compared to the base NOTSALT scenario. In the area of the salt ridge top (location 1) the positive temperature anomaly of the salt is between 7 °C (MIN scenario) and 17 °C (XTRM scenario). For all scenarios, the temperature distribution closely matches the relief of the top salt surface as depicted in Fig. 3b. Additionally within each individual scenario we can consistently observe a temperature difference of circa 20 °C between the highest and the lowest temperature at the same depth. Therefore, this temperature difference stems from the thickness difference in the salt lithostratigraphic interval. The fact that this observation is consistent in all scenarios highlights the importance of the salt layer thickness and its higher heat conductivity in shaping the temperature field.

However, the highest temperature difference does not strictly correlate with the thickest salt (located in the western part of the model) for a given depth level. The shape of the dome there is narrower hence the heat accumulation is not as concentrated as in the elongated, conical shape part of the structure in the centre of the domain. Although the effect of salt thickness is apparent, the geometrical characteristics of salt structures are also of importance. Therefore thickness alone is not sufficient to predict the temperature field around salt bodies. This could also explain the differences in temperature levels presented here in comparison with previous work [31], where differences of 17.5 °C were observed between the top of a salt structure with similar thickness and the surroundings that were undisturbed by the salt intrusion. Nonetheless, deriving a generalized relation between salt thickness and temperature differences would require a systematic examination of an ensemble of salt structures.

Fig. 8 depicts the temperature difference on a N-S section (see also Fig. 7) between the resulting temperature fields of different scenarios. The MED and the NOTSALT scenario differ only in the salt layer thermal conductivity (Fig. 8d), while the other differences (between XTRM-NOTSALT and MAX-MIN) have different heat conductivity in all layers (Fig. 8e&f respectively). For all plots the temperature difference between the scenarios is zero at the top and base of the model since the same boundary conditions apply.

The only difference between the MED and the NOTSALT scenario is the heat conductivity of the salt and therefore temperature distribution dissimilarities are solely attributed to this difference (Fig. 8d). The temperature contours stop following the geometry of the Rotliegend basement around a salt layer thickness of just below 600 m (Fig. 8a). From there on, the heat anomaly is sharply centred around the contact of the top salt, increasing with thickness.

The difference between the XTRM and NOTSALT scenario is a higher heat conductivity of the salt and lower for all other layers for the XTRM scenario (see also Table 2). Again the temperature difference is centred the salt layer (Fig. 8e) and become very

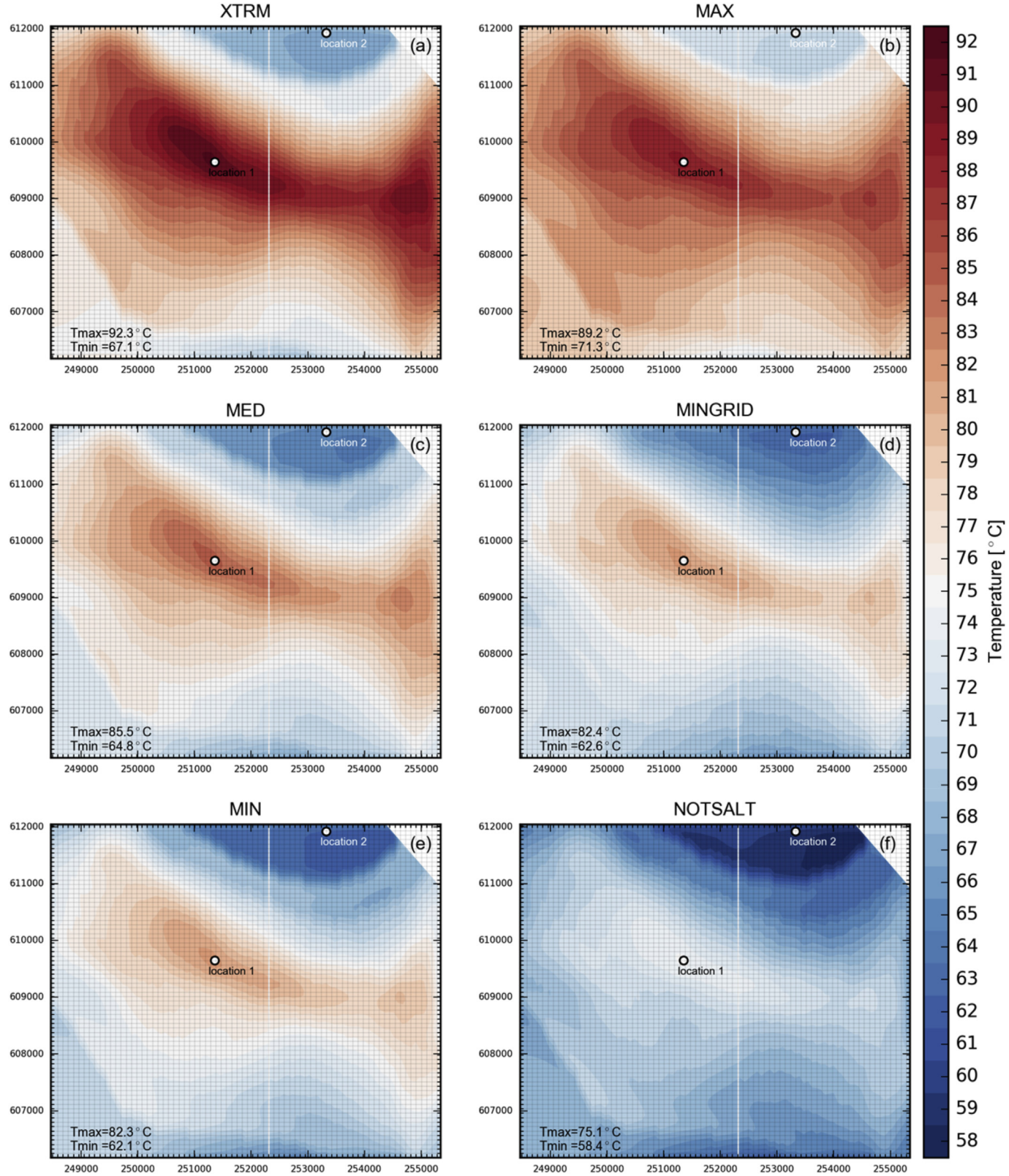

Fig. 7. Depth slice through the temperature field at 1600 m. All plots make use of the same temperature colour legend to allow cross comparison, while the minimum and maximum temperature values for each scenario are denoted on the lower left corner of each plot. The grid lines represent the simulator mesh. The marked locations represent the vertical temperature profiles shown in Fig. 6, while the white line represents the N-S section shown in Fig. 8. All scenarios make use of grid 1 except for MINGRID that makes use of grid 2 (see Table 1). (For interpretation of the references to colour in this figure legend, the reader is referred to the web version of this article.)

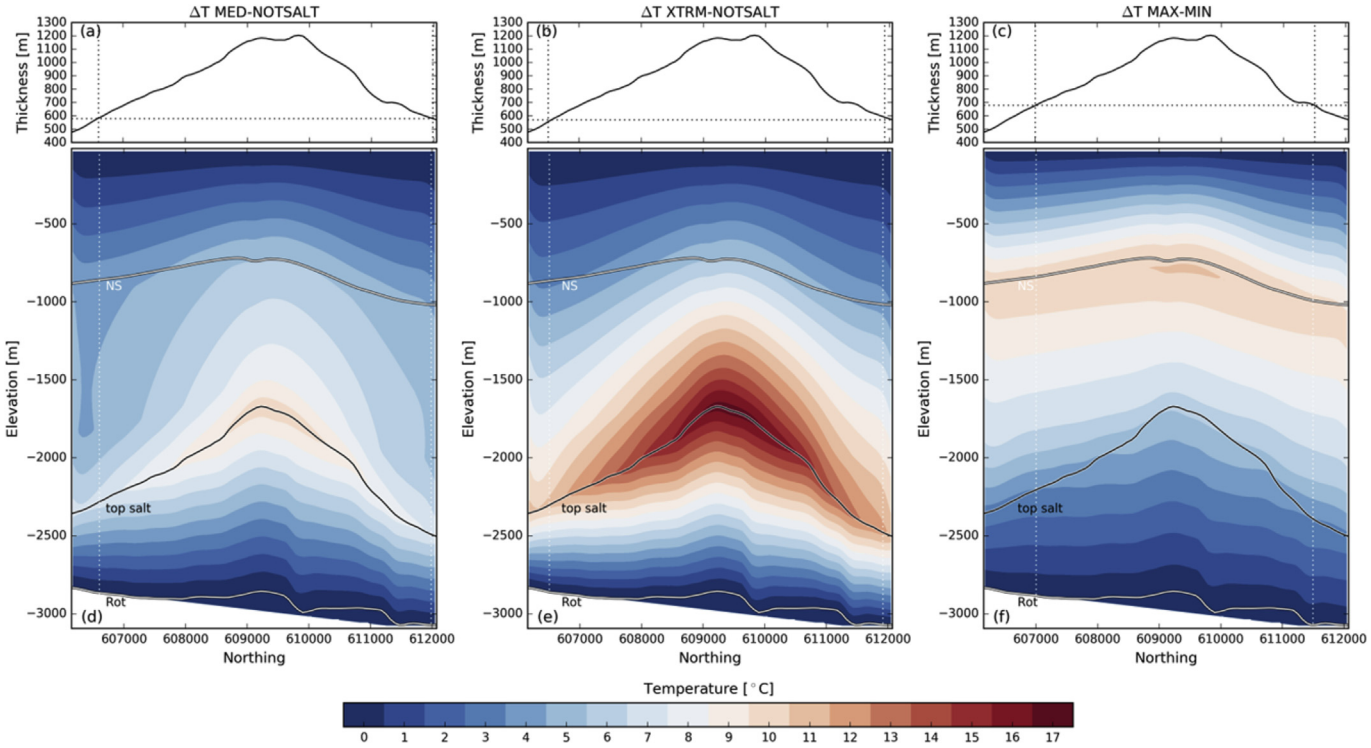

Fig. 8. Salt thickness (a), (b) and temperature difference between the XTRM and the NOTSALT scenario (c) and between the MAX and MIN scenarios (d) on a N-S section of the temperature model. The N-S section is marked as a white line in Fig. 7. The stratigraphic contacts of Rotliegend, top Salt and NS are marked.

prominent already at a thickness of about 600 m (Fig. 8b). The extent to which this heat anomaly propagates vertically beyond the salt layer is also a function of the salt thickness, since the positive heat anomaly propagates further with higher salt thickness. As a result, it is causing temperature disturbances above 10 °C, more than 700 m shallower than the top of the salt structure. The peak of the temperature difference between the two scenarios coincides with the crest of the salt structure. The effect of the heat anomaly caused by the salt is amplified compared to Fig. 8d due to the fact that the other layers have lower heat conductivity values than the NOTSALT scenario. As a result, even though the differences show similar patterns centred around salt thickness, the absolute values are higher compare to Fig. 8d.

The relative temperature difference contours between the MAX and MIN scenarios closely follow the flanks of the dome up to a thickness of circa 680 m (Fig. 8f). Above this thickness, the temperature domain is affected proportionally by the salt thickness, exhibiting a maximum difference at the top of the structure of 7 °C (see also Fig. 7). The largest difference between the two scenarios is observed around the depth of 800 m where the temperature of the MAX conductivity scenario is up to 11 °C higher than the MIN scenario. The highest temperature appears to be strongly related to the base lithostratigraphic contact of the North Sea group, which exhibits the lowest heat conductivity (Table 2) and is therefore trapping the heat below it causing a thermal blanketing effect. However, a higher temperature field could lead to higher temperatures observed at surface level, making the application of the surface boundary less realistic.

The differences between the scenarios demonstrate a consistency in their results, meaning that temperature field differences of similar level correlate to similar salt thickness (Fig. 8a,b&c). Consequently salt thickness is the causal mechanism for the temperature field differences, even though the thickness levels are not perfectly matching.

4.2. Dynamic reservoir simulations

The temperature of the middle reservoir layer for all different conductivity and production scenarios is depicted in Fig. 9. The temperature levels of the undisturbed surroundings are dictated by the respective conductivity scenario used as input (see Table 2). The cold front propagation between production scenarios shows very similar patterns, but the front propagates progressively further moving from the XTRM to the NOTSALT conductivity scenarios (top to bottom) for the same production level. Nonetheless, the XTRM scenarios generate circa 40% more energy than the NOTSALT scenario for the same flow rates and about 19% more energy compared to the MIN scenarios. These results are in accordance with a previous parametric study of thermal conductivity effects on power output [45]. Lastly, comparing the mean power generated between the MIN and the NOTSALT scenarios, we see an average increase of about 17%. These findings are in line with previous research where only the initial temperature domain in which the field is situated is important and the thermal conductivity itself appears to be insignificant [41].

Producer well temperature shows a decline analogous to the production scenario (Fig. 10), for all conductivity scenarios. The NOTSALT scenario is able to recover the original temperature of any production scenario faster than the other conductivity scenarios. With the exception of the MAX scenario and regardless of the production level, the higher the initial temperature is the longer it takes for the reservoir to recover. The largest differences occur between the XTRM and NOTSALT scenarios and are 14 years (+12%) for the lower production level and 20 years (+13%) for the highest one. The fact that the MAX scenario recovers its initial temperature faster than the MED one, could be attributed to the higher conductivity of all formations including the reservoir itself. The higher heat conductivity helps the available heat to be redistributed faster, leading to a shorter recovery time, a process that has also been

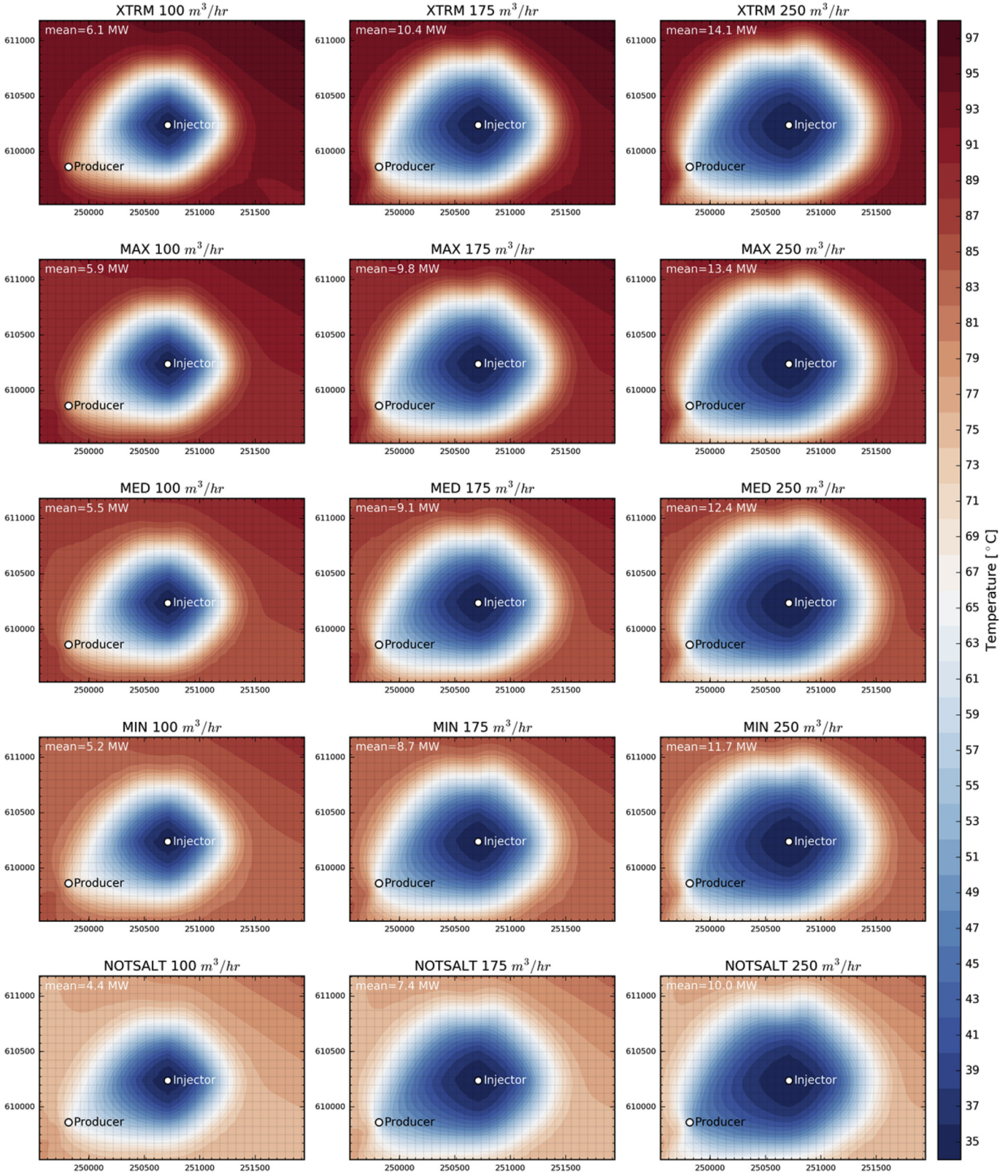

Fig. 9. Temperature maps of the middle reservoir layer at time t = 50years (end of production). All plots make use of the same temperature colour legend to allow cross comparison and the mean thermal power over the production period is denoted per plot. (For interpretation of the references to colour in this figure legend, the reader is referred to the web version of this article.)

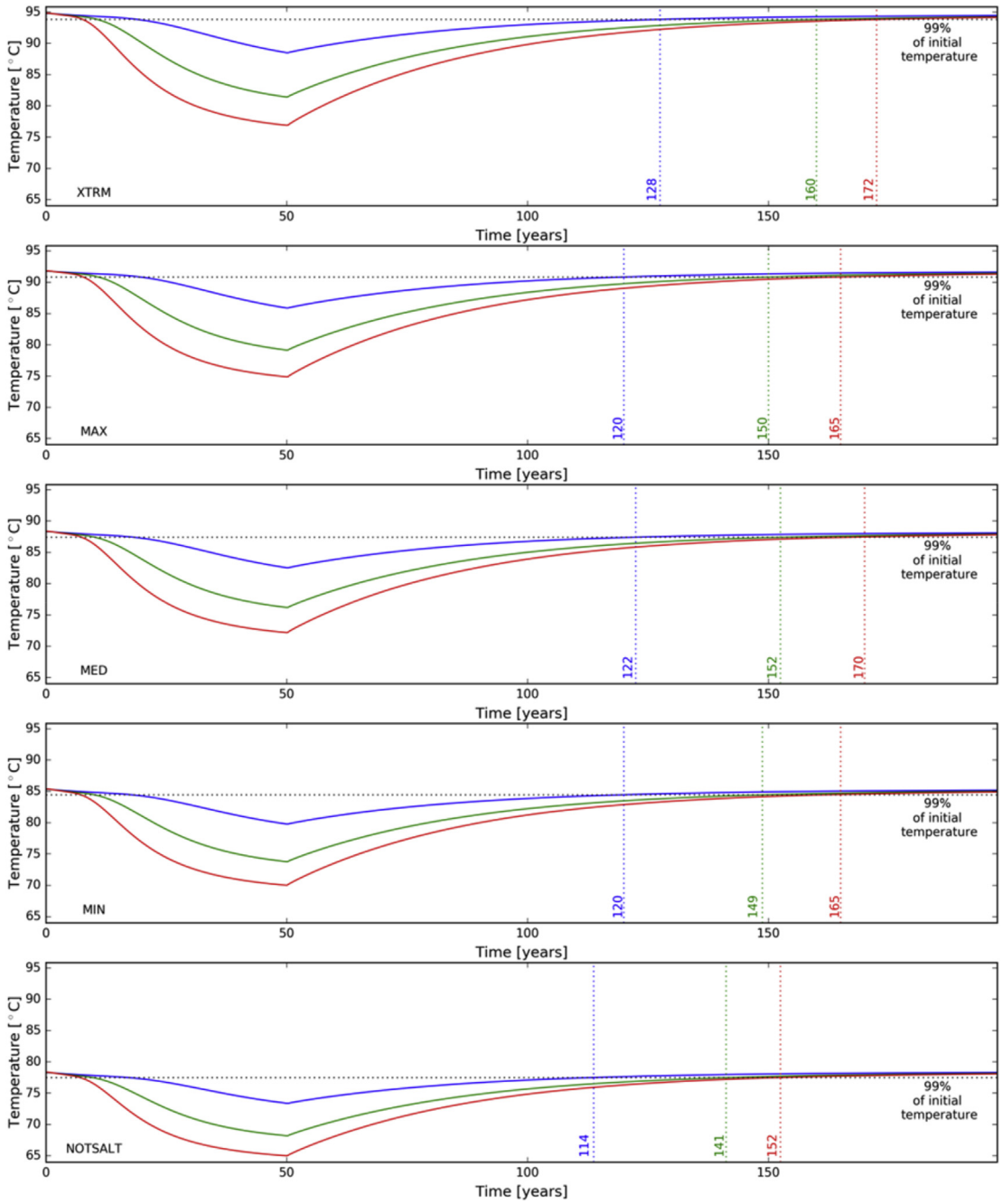

Fig. 10. Producer temperature for all heat conductivity and production scenarios. The horizontal dashed line marks the level of 99% of the initial temperature. Blue, green and red lines designate a production flow rate of 100m^3/hr, 175m^3/hr and 250m^3/hr respectively. The vertical dashed lines mark the time at which the respective production scenario has recovered its original heat level by 99%. (For interpretation of the references to colour in this figure legend, the reader is referred to the web version of this article.)

described for different geothermal applications [46]. The recovery period of the XTRM scenario is on average ~13% longer compared to the NOTSALT scenario, but the extracted energy is about 40% more. Accordingly, there is almost no difference in the recovery time between MAX and MIN scenarios, while the extracted energy is about 13% higher for the MAX scenario for the same drilling depth.

4.3. Possible applications and implications

In several locations, especially in the North East Netherlands (particularly the provinces of Groningen and Drenthe), salt thickness exceeds 800 m (Fig. 11). In light of the results presented, these locations could potentially make use of the increased heat flow of the salt for geothermal applications. Recoverable amounts of energy in these areas would be higher and at the same time the drilling depth required would be around 500 m shallower compared to a location without salt structures for achieving similar temperature levels. However, there needs to be an appropriate permeable aquifer above the salt structure. Accordingly, site specific studies should be performed to quantify the available thermal energy amounts to be extracted [47] in these potential interest areas.

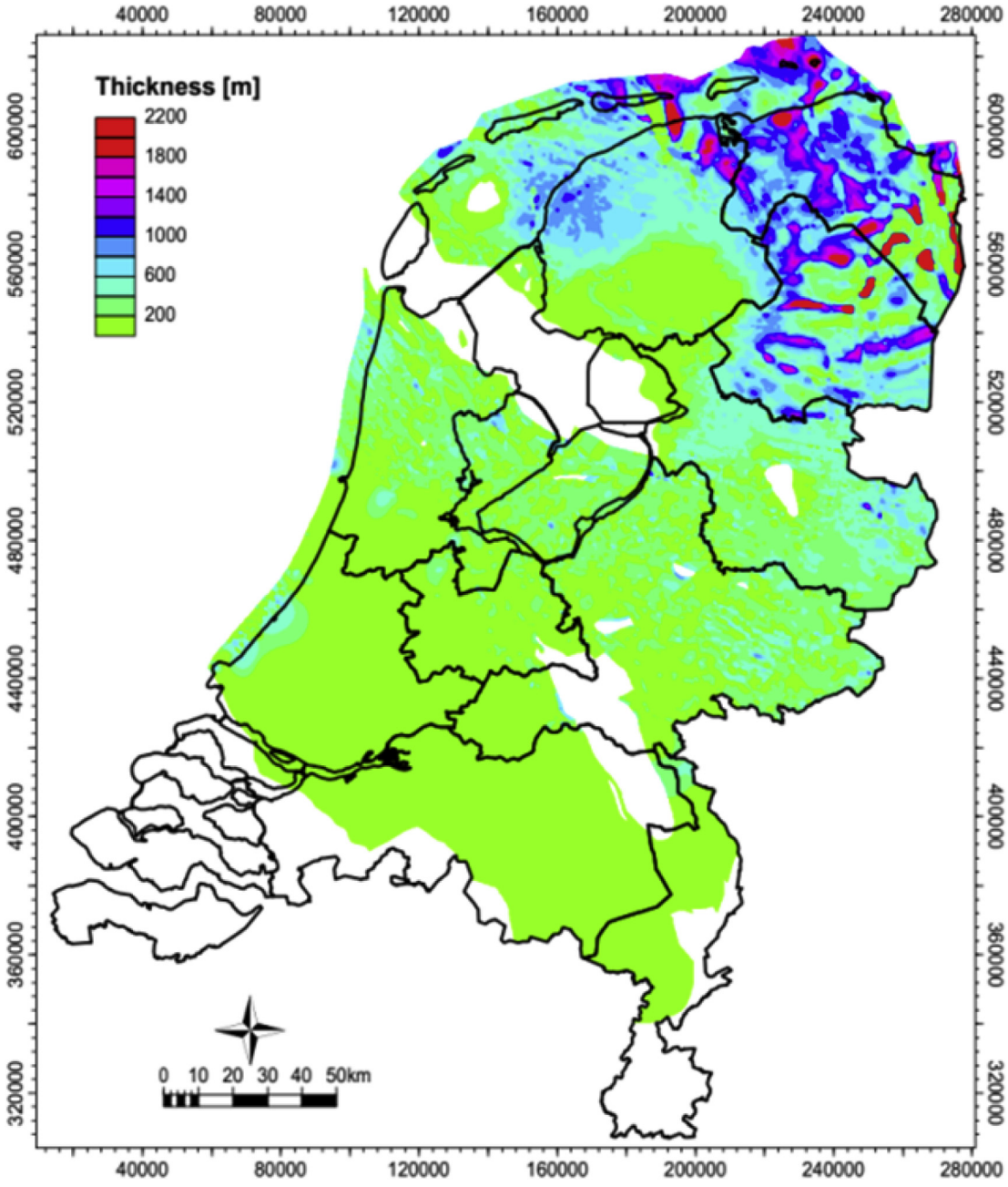

Fig. 11. Thickness of the Zechstein layer in the Netherlands. Data source: Dinoloket [48].

5. Conclusions

In this analysis, a new target for geothermal exploration is outlined. Anomalously high geothermal gradients within sedimentary basins in conductive environments can be caused by the increased thermal conductivity of salt. The associated variations in temperature gradients are proportional to the thickness of the salt but this is not the sole contributor to these higher temperature levels. The shape of the salt intrusion is also important.

Five different conductivity scenarios are considered for which the resulting temperature field is analyzed; the results are compared with DTS data from the nearby ZRP-3A well. The analysis reveals a temperature increase between 17 °C and 25 °C for the same depth between locations with normal stratigraphic salt thickness and those at the top of the salt structure.

The aforementioned differences in temperature levels correspond to a depth of 500 m–600 m for the same thermal conductivity scenario. Therefore, these higher temperatures at the top of the salt structure can be more economically reached via drilling. Consequently, the financial feasibility of geothermal projects in conduction dominated settings can be improved.

Moreover, the combination of a sandstone body atop a salt structure is substantiated as a proof of concept for direct use geothermal production. Three production scenarios are evaluated in terms of doublet performance within the aforementioned temperature fields. The considered production scenarios show a range of up to 40% more energy extracted. The resulting increased energy causes only a 13% longer recovery time in the field.

As a continuation of these findings, an economic analysis to quantify the financial benefits from the avoided drilling depth could be envisioned. Furthermore, in the locations where substantial salt thickness (>800 m) is present (e.g. the provinces of

Drenthe and Groningen), specific studies could identify the presence of a suitable aquifer for geothermal production. Lastly, the overlap between the presence of thick salt layers, a suitable aquifer and demand for geothermal heat could outline favorable locations for geothermal development. The principle can be appropriate for any geological setting that exhibits thick salt sequences or doming and interest for geothermal energy is present.

Acknowledgements

This research was supported by the research grant Flexiheat (Ministerie van Economische Zaken, Landbouw en Innovatie). The authors would further like to acknowledge Nederlandse Aardolie Maatschappij BV (NAM, a Shell operated 50-50 joint venture with ExxonMobil) for providing the 3D seismic data and the ZRP-3A DTS data, as well as Schlumberger for the academic Petrel license. Lastly we wish to acknowledge Mariene Gutierrez Neri (EBN) and Marinus de Hartogh (AKZO) for their input that helped in shaping this work.

Appendix A

List of wells used: Uithuizermeeden (UHM) cluster, Uithuizen (UHZ-01), De Hond (HND-01), Bierum (BIR) cluster, Farmsum (FRM) cluster, Delfzijl (DZL) cluster, Borgsweer (BRW) cluster, Amsweer (AMR) cluster, 't Zand (ZND) cluster.

References

[1] Alberg Østergaard P, Mathiesen BV, Möller B, Lund H. A renewable energy scenario for Aalborg Municipality based on low-temperature geothermal heat, wind power and biomass. Energy 2010;35:4892–901.
[2] Atlason RS, Unnthorsson R. Hot water production improves the energy return on investment of geothermal power plants. Energy 2013;51:273–80.
[3] Mathiesen BV, Lund H, Connolly D. Limiting biomass consumption for heating in 100% renewable energy systems. Energy 2012;48:160–8.
[4] Barbier E. Geothermal energy technology and current status: an overview. Renew Sust Energ Rev 2002;6:3–65.
[5] Goldstein B, Hiriart G, Bertani R, Bromley C, Gutierrez-Negrin L, Huenges E, et al. Geothermal energy, in: IPCC special report on renewable energy sources and climate change mitigation. 2011.
[6] Johnston IW, Narsilio GA, Colls S. Emerging geothermal energy technologies. KSCE J Civ Eng 2011;15:643–53.
[7] Beckers KF, Lukawski MZ, Anderson BJ, Moore MC, Tester JW. Levelized costs of electricity and direct-use heat from Enhanced Geothermal Systems (vol. 6, 013141, 2014). J Renew Sustain Energy 2014;6:059902.
[8] van Wees JD, Kronimus A, van Putten M, Pluymaekers MPD, Mijnlieff H, van Hooff P, et al. Geothermal aquifer performance assessment for direct heat production—Methodology and application to Rotliegend aquifers. Neth J Geosciences-Geologie en Mijnbouw 2012;91:651.
[9] Geluk MC, Paar WA, Fokker P. Salt. In: Wong TE, Batjes DAJ, de Jager J, editors. Geology of The Netherlands. Amsterdam, Netherlands: Royal Dutch Academy of Arts and Sciences; 2007. p. 279–90.
[10] Daniilidis A, Doddema L, Herber R. Risk assessment of the Groningen geothermal potential: from seismic to reservoir uncertainty using a discrete parameter analysis. Geothermics 2016;64:271–88.
[11] Trumpy E, Botteghi S, Caiozzi F, Donato A, Gola G, Montanari D, et al. Geothermal potential assessment for a low carbon strategy: a new systematic approach applied in southern Italy. Energy 2016;103:167–81.
[12] Zhang Y, Krause M, Mutti M. the formation and structure evolution of Zechstein (upper permian) salt in northeast german basin: a review. Open J Geol 2013;03:411–26.
[13] Strozyk F, Urai JL, van Gent H, de Keijzer M, Kukla PA. Regional variations in the structure of the Permian Zechstein 3 intrasalt stringer in the northern Netherlands: 3D seismic interpretation and implications for salt tectonic evolution. Interpretation 2014;2. SM101–17.
[14] de Jager J, Geluk MC. Petroleum geology. In: Wong TE, Batjes DAJ, de Jager J, editors. Geology of The Netherlands. Amsterdam, Netherlands: Royal Netherlands Academy of Arts and Sciences; 2007. p. 241–64.
[15] van Gent HW, Back S, Urai JL, Kukla PA, Reicherter K. Paleostresses of the Groningen area, The Netherlands—Results of a seismic based structural reconstruction. Tectonophysics 2009;470:147–61.
[16] Pollack HN, Hurter SJ, Johnson JR. Heat-flow from the earths interior - analysis of the global data Set. Rev Geophys 1993;31:267–80.
[17] Moeck IS. Catalog of geothermal play types based on geologic controls. Renew Sustain Energy Rev 2014;37:867–82.
[18] Scheck-Wenderoth M, Cacace M, Maystrenko YP, Cherubini Y, Noack V, Kaiser BO, et al. Models of heat transport in the central european basin system: effective mechanisms at different scales. Mar Pet Geol 2014;55:315–31.
[19] Ondrak R, Wenderoth F, Scheck M, Bayer U. Integrated geothermal modeling on different scales in the Northeast German basin. Geol Rundsch 1998;87:32–42.
[20] Noack V, Scheck-Wenderoth M, Cacace M, Schneider M. Influence of fluid flow on the regional thermal field: results from 3D numerical modelling for the area of Brandenburg (North German Basin). Environ Earth Sci 2013;70:3523–44.
[21] Agemar T, Schellschmidt R, Schulz R. Subsurface temperature distribution in Germany. Geothermics 2012;44:65–77.
[22] Nagihara S, Sclater J, Beckley L, Behrens EW, Lawver LA. High heat flow anomalies over salt structures on the Texas Continental Slope, Gulf of Mexico. Geophys Res Lett 1992;19:1687–90.
[23] Petersen K, Lerche I. Quantification of thermal anomalies in sediments around salt structures. Geothermics 1995;24:253–68.
[24] Nagihara S. Three-dimensional inverse modeling of the refractive heat-flow anomaly associated with salt diapirism. AAPG Bull 2003;87:1207–22.
[25] Cacace M, Kaiser BO, Lewerenz B, Scheck-Wenderoth M. Geothermal energy in sedimentary basins: what we can learn from regional numerical models. Chem Der Erde-Geochemistry 2010;70:33–46.
[26] Mello UT, Karner GD, Anderson RN. Role of salt in restraining the maturation of subsalt source rocks. Mar Pet Geol 1995;12:697–716.
[27] Vizgirda J, O'Brien JJ, Lerche I. Thermal anomalies on the flanks of a salt dome. Geothermics 1985;14:553–65.
[28] Zielinski GW, Poprawa P, Szewczyk J, Grotek I, Kiersnowski H, Zielinski RLB. Thermal effects of Zechstein salt and the early to middle jurassic hydrothermal event in the central polish basin. AAPG Bull 2012;96:1981–96.
[29] Bonté D, Van Wees JD, Verweij JM. Subsurface temperature of the onshore Netherlands: new temperature dataset and modelling. Neth J Geosciences-Geologie en Mijnbouw 2012;91:491–515.
[30] Kaiser BO, Cacace M, Scheck-Wenderoth M. 3D coupled fluid and heat transport simulations of the Northeast German Basin and their sensitivity to the spatial discretization: different sensitivities for different mechanisms of heat transport. Environ Earth Sci 2013;70:3643–59.
[31] Magri F, Littke R, Rodon S, Bayer U, Urai J. Temperature fields, petroleum maturation and fluid flow in the vicinity of salt domes. In: Littke R, Bayer U, Gajewski D, Nelskamp S, editors. Dynamics of complex intracontinental basins. The central european basin system. Berlin Heidelberg: Springer-Verlag; 2008. p. 323–44.
[32] Nlog. Netherlands oil and gas portal (NLOG) - boreholes. 2014. p. 2015.
[33] Maystrenko Y, Bayer U, Scheck-Wenderoth M. Structure and evolution of the Glueckstadt Graben due to salt movements. Int J Earth Sci 2005;94:799–814.
[34] Geluk MC. Permian. In: Wong TE, Batjes DAJ, de Jager J, editors. Geology of The Netherlands. Amsterdam, Netherlands: Royal Dutch Academy of Arts and Sciences; 2007. p. 63–83.
[35] Pharaoh TC, Dusar M, Geluk MC, Kockel F, Krawczyk CM, Krzywiec P, et al. Tectonic evolution. In: Doornenbal JC, Stevenson A, editors. Petroleum geological atlas of the southern Permian Basin area, houten. The Netherlands: EAGE Publications b.v.; 2010.
[36] Rockware. PetraSim. 2014.
[37] NAM. Personal communication: temperature map at the top of the Rotliegend in the area of the Groningen gas field. 2015.
[38] Norden B, Förster A, Balling N. Heat flow and lithospheric thermal regime in the Northeast German Basin. Tectonophysics 2008;460:215–29.
[39] Fuchs S, Förster A. Rock thermal conductivity of mesozoic geothermal aquifers in the northeast german basin. Chem Erde - Geochem 2010;70(Supplement 3):13–22.
[40] Noack V, Scheck-Wenderoth M, Cacace M. Sensitivity of 3D thermal models to the choice of boundary conditions and thermal properties: a case study for the area of Brandenburg (NE German Basin). Environ Earth Sci 2012;67:1695–711.
[41] Mottaghy D, Pechnig R, Vogt C. The geothermal project Den Haag: 3D numerical models for temperature prediction and reservoir simulation. Geothermics 2011;40:199–210.
[42] Magri F, Bayer U, Maiwald U, Otto R, Thomsen C. Impact of transition zones, variable fluid viscosity and anthropogenic activities on coupled fluid-transport processes in a shallow salt-dome environment. Geofluids 2009;9:182–94.
[43] Carlson MR. Practical reservoir simulation: using, assessing, and developing results. PennWell Books; 2003.
[44] Hermans T, Nguyen F, Robert T, Revil A. Geophysical methods for monitoring temperature changes in shallow low enthalpy geothermal systems. Energies 2014;7:5083–118.
[45] Poulsen SE, Balling N, Nielsen SB. A parametric study of the thermal recharge of low enthalpy geothermal reservoirs. Geothermics 2015;53:464–78.
[46] Templeton JD, Ghoreishi-Madiseh SA, Hassani F, Al-Khawaja MJ. Abandoned petroleum wells as sustainable sources of geothermal energy. Energy 2014;70:366–73.
[47] Procesi M, Buttinelli M, Pignone M. Geothermal favourability mapping by advanced geospatial overlay analysis: tuscany case study (Italy). Energy 2015;90(Part 2):1377–87.
[48] Dinoloket. Digital geological model (DGM) v.4. 2014. p. 2016.